Fiber link design for the NASA-NSF Extreme Precision Doppler Spectrograph concept "WISDOM"

Gábor Főrész [a], Rafal Pawluczyk [b], Paul Fournier [b], Robert Simcoe [a], and Deborah F. Woods [c]

[a] MIT Kavli Institute for Astrophysics and Space Research, 77 Mass. Ave, Cambridge, MA 02139, United States;
[b] FiberTech Optica (Canada);
[c] MIT Lincoln Laboratory (United States).
contact: gfuresz@mit.edu

ABSTRACT

We describe the design of the fiber-optic coupling and light transfer system of the WISDOM (WIYN Spectrograph for DOppler Monitoring) instrument.   As a next-generation Precision Radial Velocity (PRV) spectrometer, WISDOM incorporates lessons learned from HARPS about thermal, pressure, and gravity control, but also takes new measures to stabilize the spectrograph illumination, a subject that has been overlooked until recently.   While fiber optic links provide more even illumination than a conventional slit, careful engineering of the interface is required to realize their full potential. Conventional round fiber core geometries have been used successfully in conjunction with optical double scramblers, but such systems still retain a memory of the input illumination that is visible in systems seeking sub-m/s PRV precision. Non-circular fibers, along with advanced optical scramblers, and careful optimization of the spectrograph optical system itself are therefore necessary to study Earth-sized planets. For WISDOM, we have developed such a state-of-the-art fiber link concept. Its design is driven primarily by PRV requirements, but it also manages to preserve high overall throughput.

Light from the telescope is coupled into a set of six, 32 μm diameter octagonal core fibers, as high resolution is achieved via pupil slicing. The low-OH, step index, fused silica, FBPI-type fibers are custom designed for their numerical aperture that matches the convergence of the feeding beam and thus minimizes focal ratio degradation at the output. Given the demanding environment at the telescope the fiber end tips are mounted in a custom fused silica holder, providing a perfect thermal match. We used a novel process, chemically assisted photo etching, to manufacture this glass fiber holder.

A single ball-lens scrambler is inserted into the 25m long fibers. Employing an anti-reflection (AR) coated, high index, cubic-zirconia ball lens the alignment of the scrambler components are straightforward, as the fiber end tips (also AR coated) by design touch the ball lens and thus eliminate spacing tolerances. A clever and simple opto-mechanical design and assembly process assures micron-level self-alignment, yielding a ~87% throughput and a scrambling gain of >20,000.

To mitigate modal noise the individual fibers then subsequently combined into a pair of rectangular fibers, providing a much larger modal area thanks to the 34x106 micron diameter. To minimize slit height, and thus better utilize detector area, the octagonal cores are brought very close together in this transition. The two outer fibers are side polished at one side, into a D-shaped cladding, while the central fiber has a dual side polish. These tapered, side-flattening operations are executed with precise alignment to the octagonal core. Thus the cores of the 3 fibers are brought together and aligned within few microns of each other before spliced onto the rectangular fiber.

Overall throughput kept high and FRD at bay by careful management of fiber mounting, vacuum feed-through, application of efficient AR coatings, and implementation of thermal breaks that allow for independent expansion of the fibers and the protective tubing.

Keywords: precision radial velocity spectrograph, pupil slicer, double scrambler, non-circular fiber geometry, near field, far field, focal ratio degradation, scrambling gain, PRV, TESS, FRD

1. OVERVIEW

1.1 Project background, requirements and design choices

Precision radial velocity (PRV) follow-up is a very important part, and a real bottleneck, in supporting transiting exoplanet surveys. Based on lessons learnt from Kepler and in anticipation of the upcoming TESS mission, a NASA-NSF collaboration 'NN-EXPLORE' set out to build a new and much needed PRV facility for the astronomical U.S. community. Given that the TESS experimental design is most sensitive to planets in short (<30 days) orbits, and thus will provide candidates with low RV amplitudes, the call for proposals designing this new instrument asked for an Extreme Precision Doppler Spectrograph

(EPDS) that aims to reach "0.5m/s precision as a requirement with a 0.1m/s goal, without astrophysical noise". The adjective *extreme* comes from the current state of PRV instrumentation, where seems to be a ~1m/s observational precision barrier[1]. This is partially imposed by instrument systematics and, in probably larger part, by astrophysical noise of the target stars. Since we only have fairly limited control over the latter (by selecting inactive and very quite stars) we interpreted the NN-EXPLORE announcement of opportunity as pushing the instrument design to the extreme and thus aiming to improve on the current state of the art.

PRV instrumentation and data reduction techniques have became so refined by today that there remains no single obvious path to move forward[2]. Thus in our response to the EPDS call the WISDOM design[3] (WIYN Spectrograph for DOppler Monitoring), while building on well established heritage and incorporating best practices, have addressed improvements of many PRV instrument subsystems. If there is one area, though, in which ways of improvements are not yet fully explored that is very cautious optical design and careful illumination control of the spectrograph. Our papers on WISDOM[3] and its optical design[4] elaborate on the former, while this paper is mainly concentrating on the latter, by describing a fiber optic link that is designed to provide high throughput and a very uniform, stable spectrograph illumination.

Iodine-cell based PRV systems are inherently less sensitive to changes of spectrograph illumination, as the calibration and stellar spectra are recorded truly simultaneously and both experience the exact same optical path through the atmosphere and spectrograph. However, these systems have a fairly limited passband (500-600nm) and therefore access a relatively small subset of spectral lines, thus the achievable RV precision is constrained. Since the EPDS call specified 0.5m/s or better precision as a requirement we thought that an extended wavelength range, and therefore access to more RV content within such extended passband, is highly desired. Given the importance of M-dwarfs in the TESS sample[5] and the likely ability to better mitigate stellar jitter by comparing near-infrared (NIR) RV values to results based on the visible spectrum[2] we opted for a relatively wide wavelength coverage of 380-1300nm. This is similar in approach to that of CARMENES[6], although not taking the red cutoff beyond the J band allowed us to significantly simplify the instrument design. Still, we decided to split the VIS-NIR coverage into a "Short" and "Long" passband spectrograph. Each of these channels is fed by individual fiber links, simultaneously illuminated at the telescope front end after a dichroic (at 750nm) split before the fiber entrances[3].

1.2 Essential components of a PRV fiber run

Essentially every spectral line is a monochromatic image of the spectrograph entrance slit. Therefore if the illumination of the slit changes during (or between) exposures that directly maps into variations of the line profiles (or line spread function, LSF), often resulting in a shift of the line centroid and/or distorting the line bisector. Stellar activity, e.g. spots on a rotating stellar surface, can have similar effects. So in order to be able to distinguish stellar jitter from instrumental effects, and to deduce the real RV signal imposed on the star by the planet, it is highly desired to have a stable slit illumination. Such stability of the "near field" is the Achilles heel of slit fed instruments where guiding errors move the star within the slit jaws and introduce time dependent changes of the LSF. (Unless an iodine cell is used, but as mentioned above that inherently limits the achievable RV precision.) Scrambling, the huge number of bounces light experiences within an optical fiber, efficiently erases any first order structure that filters through from intensity distribution changes at the fiber entrance[7]. However, the illumination at the fiber output face is not completely even since in circular core fibers the internal reflections are not entirely random. While scrambling in the azimuthal direction is efficient, information about the input conditions is often preserved in the radial sense, as it has been well documented by the literature[7,8]. Non-circular core geometries inherently increase the near field scrambling[8,9], and so many modern fiber runs use octagonal fibers as their shape closely resembles the circularly symmetric seeing limited image of a star at the telescope focal plane. (Or in case of pupil feed, which is an alternative method coupling light into the fiber, the also circular pupil image of the telescope primary gets projected onto the fiber end face.)

It is important to note, however, that at the m/s and sub-m/s level the near-field scrambling of even the non-circular fibers are insufficient by themselves, and thus effects of the telescope (guiding) and the atmosphere (dispersion, seeing at some extent) should be actively minimized. Fast acting (10-100 Hz) tip-tilt systems and atmospheric dispersion compensators are a must, while a low order adaptive optics system can be beneficial to increase throughput. Higher order AO systems, if available, can significantly decrease the overall size of the instrument (as Eq. 1 further below describes it). Although it is often large telescopes (6-10m) that are equipped with such facility – but it is usually smaller telescopes that can commit much larger fraction of the observing time to a given program, which PRV observations really need and can significantly benefit from. For those smaller (2-4m) telescopes an AO system is rarely an option, but in the absence of AO pupil or image slicing can be used to decrease the instrument size and thus the overall budget (see section 2.1, [3]).

Distortions of the LSF can also be a consequence of illumination variation across the spectrograph pupil, or as it is referred to the "far field". Stronger illumination at the edge of powered optical elements weigh aberrations more heavily into the point spread function (PSF) of the optical system, and this could, in a complex and wavelength dependent way, affect the

line centroids and thus result in instrumental RV errors[10,11]. Since fibers, even non-circular core ones, do not scramble the far field sufficiently[9], an optical double scrambler[12] is often employed within a PRV fiber run. Although it often comes at a price of a throughput hit[13], PRV observations benefit more from resolution than S/N ratio[14] as former is set and usually fixed within an instrument while latter can be improved/regained by longer integration times.

Modern PRV spectrographs are often housed within tightly controlled environments and the fiber link has to penetrate through a vacuum vessel. Optical relay systems can be a solution[15], also serving as the realization of a double scrambler. The issue could be the relative alignment between the vacuum-vessel-mounted fiber end on the outside and on the inside. These need to be kinematically mounted and 'decoupled' from the vessel in a way that the vessel can change its shape (which occurs due to ambient pressure variations) without misaligning these two optics respect to each other. Embedding the optical fiber cable itself in some sealed feed-through connector avoids this problem, also likely offers higher throughput – although stress induced in the feed-through can increase focal ration degradation (FRD) and thus still affect efficiency.

Ultra stable calibration sources with high line densities and proper calibration light injection is a critical component to a PRV instrument. State of the art laser frequency combs (LFCs) have the ideal properties in terms of high and very even line density, along with high intensity and cm/s level long term stability[16], although still cannot span the entire passband of many spectrographs. But such calibration sources are inherently coherent, which leads to the rise and importance of modal noise, the variation in the apparent interference pattern of the possible light propagation modes within the fiber. This is less of an issue for the non-coherent starlight, but time dependency of modal structure (due to temperature, pressure changes and movement of the fiber) and its strong presence in coherent calibration light can result in a systematically offset wavelength reference and thus instrumental RV errors. Mitigation of modal noise therefore is important, that is usually achieved by introducing phase shift between the modes via simple mechanical agitation[17] (10-100Hz shaking). This, over long period of time might affect the mechanical integrity and FRD properties of fibers, and so acoustic modulation (periodic increase of air pressure around the fiber) could be a viable alternative.

In summary the key components of a PRV fiber run in our WISDOM design are: pupil slicing; use octagonal fibers; an efficient, high throughput double scrambler; modal noise suppression and mitigation techniques; low FRD vacuum feed-through and overall low stress fiber mounting and handling; and common path calibration light injection. In Section 2 we discuss most of these elements in more detail.
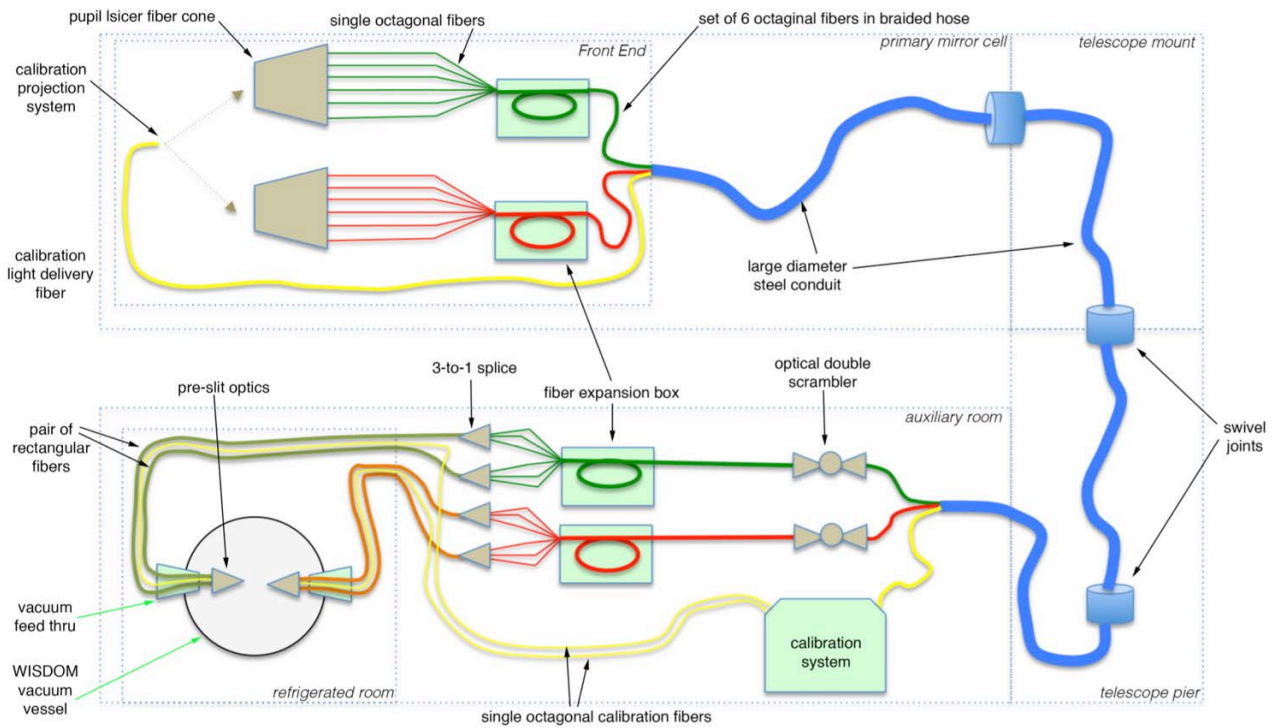

Figure 1. Schematic of the fiber-optic link. Light at the front end is split via a dichroic into the SWA and LWA, which feed two identical pupil slicers of six fibers each. These run through a conduit downstairs to the scrambler system, after which the twelve octagonal fibers are spliced into four rectangular cores and fed into the SWA and LWA portions of spectrograph.

2. FIBER LINK SUBSYSTEMS

Figure 1 presents a schematic overview of WISDOM's optical fiber subsystem. From each pupil slicer (Section 2.1), a sextet of octagonal fibers (Section 2.2) emerges from the fused silica fiber mounting cone, located at the slicer focus. These fiber bundles then enter protective tubing and traverse an "expansion box" that houses service loops and spare fiber. Then the fiber is re-routed into a steel-braided flexible hose. Between the Front End and the WIYN elevation disk, a weather-tight flexible steel conduit carries these hose-wrapped fiber bundles to the primary mirror cell, at which point they are directed into the telescope and pier. Inside the telescope, the fiber remains protected by conduit that adjusts with telescope pointing via swivel joints (minimizing length). In addition to the two six-fiber bundles a single fiber runs up the conduit to bring light from the downstairs calibration system to an injection point at the Front End.

In the spectrograph room the science fibers feed into optical double scramblers (Section 2.3), after which a much shorter fiber run leads into the environmentally controlled spectrograph and terminates at the slit. Along this short length, the six science fibers for each arm are arranged into two groups of three, and spliced onto a pair of rectangular fibers with 3:1 aspect ratio (Section 2.4), increasing the modal volume presented at the slit. These rectangular fibers enter a feed-through (Section 2.6) designed to minimize strain-induced FRD after which they are arranged into a pseudo-slit configuration with the two rectangular fiber ends flanking a calibration fiber that provides a simultaneous wavelength reference. A small set of injection lenses is used to re-image the fiber output from its native F/3.0 focal ratio to the F/8 and F/12.5 speeds appropriate to the SWA and LWA collimators, respectively. The run has a total length of 20-22 meters from telescope to scrambler, and 7-8 meters from scrambler to slit.
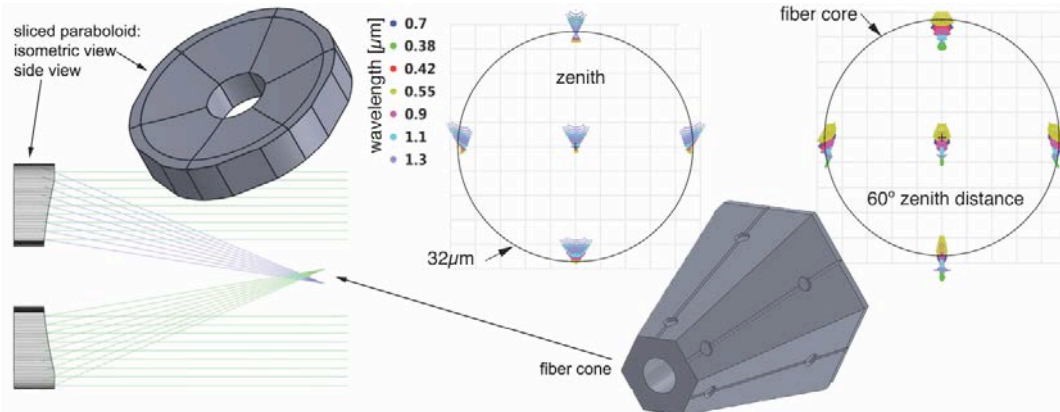

Figure 2. Ray-trace diagram (lower left) shows how the physically sliced and then recombined parabolic mirror (upper left) crosses the six focused beams (2 shown on ray trace) into fibers mounted to a fused silica six-sided cone (bottom center). The upper center displays image quality as a polychromatic spot diagram for 0, ±0.6″ field positions and an infinitely small theoretical source, overlaid on the 1.2″=32μm fiber core. Up right is a similar spot diagram but for 60° zenith distance, showing how effective the atmospheric dispersion compensator[3] is over the wide, 0.35-1.3μm passband.

2.1 Pupil Slicer

Slicer Theory

The reasoning behind the use of a pupil slicer is given in the main WISDOM paper[3], along with the Front End optical layout. The opto-mechanical realization of the pupil slicer is discussed in [18]. Here we give: a brief description of the optical design; the reasoning behind the choice of a macroscopic pupil slicer rather than a fiber-based or an image slicer; and also discuss some of the design choices and optimization process.

Re-collimating the F/6 telescope beam beyond the primary focal plane via a 450mm focal length off-axis paraboloid[3] (OAP) the front end creates a 75mm pupil image (the image of the primary mirror) on a segmented, fast paraboloid mirror that serves as the slicer. This mirror is physically cut into 6 "pizza" slices, which segments then are pushed radially inward to eliminate the gap caused by the cutting process (see Figure 2). This increases efficiency as the mirror surface becomes nearly continuous, while the mirror now creates six independent foci points. The fibers are mounted on V-grooves machined into the sides of a hexagonal fused silica cone that follows the arrangement of the foci, while the material matches the coefficient of thermal expansion (CTE) of the fibers. Lateral shifting of mirror segments[18] can precisely match the six foci locations to the as-mounted fiber end positions. As shown on Figure 2 the image quality of this purely reflective slicer is excellent and fully achromatic, and even combined with the ADC[3] the image quality is only limited by the telescope and the atmospheric seeing, not the slicer.

Slicer Optimization

The 6 foci of the slicer are at a much larger (more ″/mm) plate scale than the telescope primary focus due to demagnification between the collimator OAP and the slicer. This decreases the physical size of fibers that required to match a given angular seeing disc (φ) and as a consequence the slit width of the spectrograph narrows, or in other words this boosts the spectral resolution (R) even for the same size (D_{beam}) instrument:

$$R = \frac{2D_{beam} \tan \delta}{\phi D_{tel}} \tag{1}$$

An alternative interpretation is that the resolution boost is due to the decreased effective diameter of the telescope (D_{tel}): the slicer essentially creates six smaller telescopes that together make up for the same light collecting area as the single primary mirror but the photons captured are now distributed amongst 6 fibers which form a much longer, although narrower, slit.

To calculate the effective resolution boost we must first account for a plate scale reduction at the fiber input relative to the telescope. This is given by the ratio of the slicer mirror and OAP focal lengths, that is 450mm/110mm≈0.25 in our case. With this reduction the desired 1.2″ aperture[3] maps to 30μm physical length, rather than 120μm at the native focal plane/plate scale of WIYN. But we do not gain a resolution boost of 120μm/30μm=4 that the change in slit/fiber size would imply, because by reimaging to a larger plate scale we have also changed the focal ratio of rays entering the fiber. It's important to remember that the derivation of Equation 1 implicitly assumes equal focal ratios of the telescope and spectrograph collimator. So if the slicer changes the telescope focal ratio then a correction must be applied to properly calculate the increase of resolution. This correction factor is given as the ratio of the nominal telescope f-number (6) to the effective input focal ratio of the fiber. While a side-view ray trace diagram (Figure 2) might suggest that the fiber input focal ratio of the slicer is relatively modest at ~F/4, this is misleading. Incident angles of rays accounting for the extreme corners of each petal-shaped mirror slice are equivalent to F/2.7. Therefore we must apply a correction factor of 6.0/2.7=2.22 to our results, to preserve the validity of Eq. 1. So the resolution boost of the slicer as indicated by the plate scale change (4.0) has to be reduced by the focal ratio conversion factor (2.22), leaving a total slicer resolution boost of 4.0 / 2.2 = 1.8.

Not changing the OAP/slicer focal lengths (i.e. at a fixed plate scale reduction factor of 4.0) it is still possible to further gain some resolution by slowing down the acceptance cone of the fiber input, thus decreasing the focal ratio conversion factor. This can be done either by tailoring of the fiber numerical aperture, or equivalently masking/apodizing the slicer segments. However either one results in a throughput loss, as light from the outer parts/corners of the mirror segment do not couple into the fibers, a geometrical loss we can coin "pupil transmission". Alternatively the plate scale reduction can be changed, but then sticking to a given physical fiber size (to preserve spectral resolution) the angular coverage of the fiber will change with plate scale and that affect efficiency. This establishes a well-defined trade space between boosted resolution and throughput, which we explored. As pointed out in [14] resolution is more valuable for PRV spectrographs than throughput. While one could argue that the choice therefore is very simple, we tried to figure out if there is an optimal value for the resolution-throughput product:

Fixed plate scale, varying f-ratio. One option to tailor the feed focal ratio (and thus the exiting focal ratio) of the fibers is to place a pupil mask over the slicer mirror, which, as mentioned above, causes throughput loss. Looking at Eq. 1 this is essentially decreasing the effective size of the telescope D_{tel}, as each slicer segment gets smaller. As an alternative implementation of this we also could tailor the NA value of the fiber itself, by customizing the refractive index properties of the fiber preform, and so the fibers would not be able to "see" the edge of the slicer mirrors. (Feeding closely to their nominal NA optical fibers exhibit very low focal ratio degradation: when nearly all possible light propagation modes are excited at the fiber input then the exiting light cone is also spread nearly the same angle than that of the entrance cone of light.) So while this method also causes throughput loss, it has the advantage of minimizing FRD in the fiber itself. And as later discussed (see Eq. 2) the lower value of fiber NA makes the implementation of the scrambler less challenging.

Varying plate scale, fixed f-ratio. Looking at Eq. 1 the apparent other way to increase resolution, without altering the spectrograph, is to decrease the angular size of the slit, φ. But that is typically matched to the atmospheric seeing and lowering it comes at a price of decreasing efficiency as a smaller slit utilizes less light of a given FWHM seeing disk. For now let's fix the fiber size (=slit) at 30μm diameter and its feed focal ratio at f/3.0, and vary the plate scale of the telescope by changing the focal length of the slicer mirror (or the OAP that directs the collimated light onto the segmented slicer mirror). With shorter and shorter focal lengths of the slicer the fixed fiber covers an ever larger angular extent on the sky, thus the seeing or slit loss is decreasing. But at the same time the fixed f-ratio of the fiber is unable to gather all the light directed towards it by the faster and faster focal ratio slicer segment, resulting in an increasing geometrical loss (pupil transmission).

These two competing efficiencies are plotted on Figure 3, expressing the effective telescope diameter (left) or the "resolution boost factor" (right) of the slicer. There appears to be a clear maximum at around 1.5m effective telescope diameter, or a slicing factor of 2.33. This allows around 92% pupil transmission, and at f/3.0 a 30um fiber is 1.41″ on the sky with 76% transmission of an 0.8″ seeing disc (using a Moffat function to describe the WIYN PSF at and 0.7″ FWHM). Hence, an overall transmission of just over 70%.
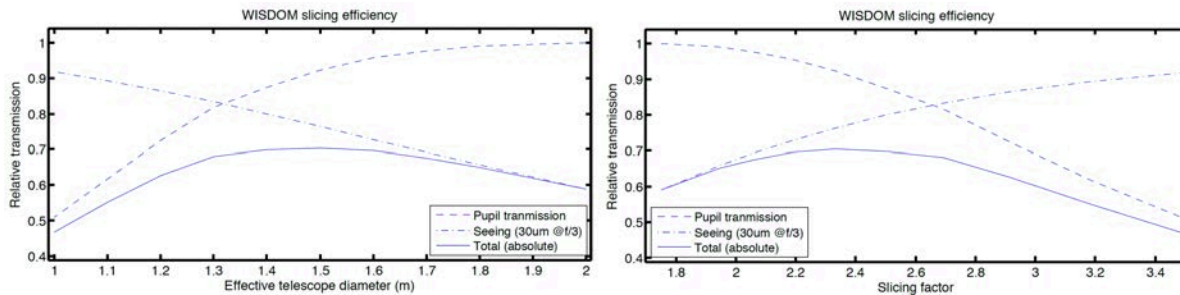
Figure 3. The competing slit and pupil efficiencies define an optimal slicing factor

As mentioned above there is some added complexity in such optimization as the fiber f-ratio also affects the single ball lens double scrambler design (see Section 2.3). Taking into account manufacturing considerations, and executing a similar trade study exploring the parameter space a bit differently (i.e. fixing the plate scale and fiber size, but varying the f-ratio of the fiber and the beam diameter) we arrived to the same conclusion: the optimal slicing or resolution boost factor is 2.33, although an f/3.5 fiber feed and a 1.2″ sky coverage using a 32μm core fiber results in a better scrambler design.

Alternative Realizations

The slicer would be subject to much more benign environmental requirements if located not at the moving telescope exposed to changing temperatures but downstream near the spectrograph, in a constant gravity and thermally controlled environment. However, at the telescope front end the center of the pupil is empty due to the shadow of the secondary. Therefore our design takes advantage of not needing a 7th, central segment, and so has relative simplicity and high efficiency.

A microscopic pupil slicer, based on a microlens array and a fiber bundle[19], would be another option but that requires much smaller opto-mechanics and it would not be necessarily simpler or cheaper. Alignment/machining tolerances would also be harder to control, and that could severely hurt the throughput. Our design also has the advantage of straightforward implementation of a fiber viewer: looking directly at the fiber ends through the central opening of the slicer mirror allows for direct feedback of fiber coupling efficiency, something that is really hard to get in a microscopic slicer.

At last we have to mention the viable choice of an image slicer, which we abandoned since we wanted to have even distribution of light amongst the fibers, in order to provide a very even slit illumination. This is very important for a PRV instrument even if, as in our case, great care had been taken to eliminate any slit tilt variations across the echellogram and the individual fibers are combined and mixed via a rectangular fiber just before the slit.

2.2 Non-circular Core Fibers

As reviewed in the introduction and further discussed in the referenced publications[7-13], non-circular fiber core geometries, especially octagonal ones, are much better at evening out the near field. Although an often-observed problem associated with such special light guides is a pronounced structure in the far field[20] (Figure 4, upper center), that is very sensitive to input conditions and movement of the fiber. The emergence of these highly undesired features is contributed to "cladding modes": To lower manufacturing cost octagonal fiber core preforms are first deposited with a thin layer of doped cladding, then ground to a round outer shape, inserted into a tightly fit glass tube which is then heat-collapsed onto the doped cladding layer to form the final preform. This outer tube forms the often un-doped secondary cladding that mainly serves as mechanical protection. This two step process saves cost as the gas-phase deposition of the fluorine doped primary cladding is very time consuming and rather expensive, thus not economical to make a large core-clad diameter ratio (CCDR).

Fiber Customization

For our 32μm cores we needed a relatively tick cladding, in order to be able to handle the fibers. Typically below 80μm it is really hard to manipulate, cleave or even polish a fiber. So we opted for a large, 1:2.2 CCDR (typical values are 1:1.2-1.3) and decided to have the vendor implement the caldding entirely by the deposition process. To our surprise this increased the cost of the custom preform by a factor of two. Since we also specified a unique NA value to match our desired F/3.5 fiber feed the cost jumped up again, bringing the total to be 3-times as expensive as a conventional preform. Almost all of this increase was claimed not by the fiber vendor but the preform manufacturer. (As discussed above the optimal pupil slicer requires a fiber feed f-ratio of F/3.5, and so allowing for 10-20% FRD to take place we specified the NA of the fiber to be 0.175 or F/2.8.) We also wanted excellent blue and simultaneously great red/NIR transmission, so chose the all-silica step index FBPI type fibers from Polymicro, and we worked with them to procure and draw our customized, octagonal fiber.

The real surprise, however, came when the fiber was delivered (after a really long lead time): despite the single cladding deposition process the near field still showed some low level structure while the far field exhibited a strong albeit strictly radial pattern (Figure 4, lower center). After some inquiries we got hold of the refractive index profile of the preform, measured by the preform vendor, and it explained everything (see Figure 4, right). Instead of a step index fiber the process resulted in a highly modulated index variation within the core, essentially creating a virtual inner cladding that severely affects the far field behavior. (Although it is still much better, more even, than it is for a dual clad fiber.) How could it happen? The answer is likely in the manufacturing process itself: The deposition of such thick cladding requires the preform core to spin on a lathe while gas torches are running up-and-down the length of it to heat the core while a doped gas mixture is aimed at the heated area. It is a slow process and thus the core is exposed to too much increased heat over a very long period of time. This causes some of the dopant to diffuse into the core and create a depleted region, which then creates the virtual secondary cladding. Determining a single NA value of our custom fiber is almost meaningless as the clad/core index ratio is constantly changing (Figure 4, right). The peak is around NA=0.258, while the minimum indicates NA=0.179, averaging to about 0.212 that fails to meet our target (0.175) and falls outside the vendor specification (0.175±0.025).
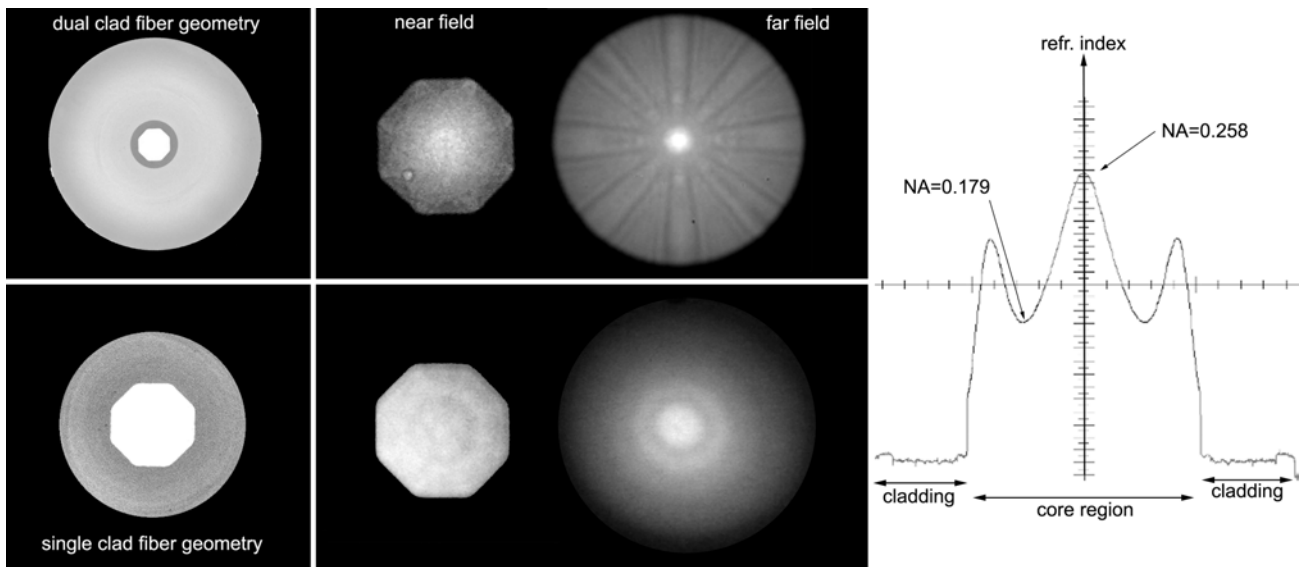

Figure 4.   Dual clad[20] (upper row) and single clad (bottom row) octagonal fiber core geometries (left) and near/far field patterns (middle). The refractive index profile of our "single clad step index" fiber is shown on the right.

The lesson learned is that any fiber customization, even if it is well within the manufacturers allowable parameter space (or so they think), can carry a risk - although it does validate our choice of ordering the fiber early on, and setting out to not just procure it but also to verify its performance. In light of the as-measured index profile another cautionary tale is that even if the NA value is known for a fiber, the actual refractive index profile is usually not available, and thus a realistic "as built" fiber could behave very differently than one would expect based on the NA value and assuming a well behaved step index profile. This emphasizes the importance of testing over simulations or simple analytic calculations, as not even beam propagation method based numerical models could have predicted the near/far field behavior of a fiber that exhibits the index profile shown in Figure 4, unless, of course, the exact profile is known. But testing is much more sufficient than such complex simulations, which is the reason why we designed and built our own comprehensive test setup (see Section 3).

2.3 Double Scrambler

As discussed in the introduction not even octagonal fibers scramble the far field sufficiently. The solution is to use a double scrambler[12] that exchanges the near- and far field between two pieces of fiber, or in other words transfer the spatial light distribution of one fiber end to angular illumination variation at the other fiber end, and vice versa. We chose the single ball lens design that, if made of a high index material, allows for simple opto-mechanics as the fibers can be simply pushed against the ball lens for axial placement and only radial alignment is needed[13]. The diameter of the optimal ball lens in such configuration is tied to the refractive index of the ball (n), the fiber diameter (d) and its NA[13]: $D \approx 2d*(n-1) / 2*NA$.
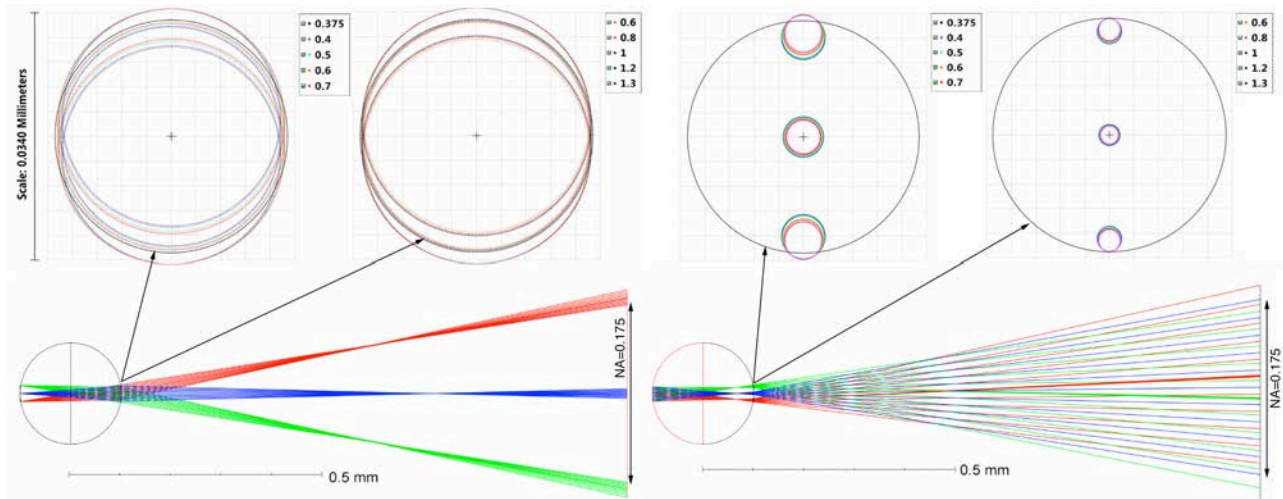
Figure 5. Ray trace of the WISDOM ball lens double scrambler, illustrating the exchange of near and far-field patterns (angular and spatial distribution), and confinement of emergent rays within the entrance face and NA of the input fiber.

However it is really only n=2 and higher index materials that results the desired zero back focal distance (BFD) configuration. For our small core diameter of 32μm and design NA of 0.175 the required ball lens diameter was 175μm (or 150μm for a standard NA of 0.22), which is too small if using LASF-35 or S-LAH79 glass (n≈2.0). Those high index materials are typically very soft and vendors indicated that the smallest feasible ball size to manufacture is 250μm.

Cubic zirconia (n=2.2) is often not considered as a viable lens material due to its poor transparency below 400nm, but for a couple hundred micron thickness it is still >98% efficient at our blue cutoff of 380nm. Due to its higher index the optimal ball size becomes 20% larger at 220μm, and being a much harder material there is no issue with manufacturing. Swiss Jewel offered 200μm off-the-shelf zirconia balls, and while a bit smaller than the ideal size these optically work well (see Figure 5) and are obtainable at a very reasonable price.

The only issue is anti-reflection (AR) coating. The scrambler design relies on the light rays exiting the fiber and enter the ball through an air gap (except the single point of contact), and at such high refractive index the Fresnel losses are very high, above 14% for the most extreme angles. There are not too many vendors who can evenly deposit AR coating on such small lenses, but Deposition Sciences offered a somewhat expensive but highly efficient coating with >98% efficiency over the 380-750nm and 750-1300nm passbands (although apparently they lost 2/3 of the ~200 small balls in the coating process, as we only received ~30 lenses of each coating). To estimate the overall throughput we used Zemax to simulate the wavelength dependent coupling efficiency that consists of inherent geometrical losses (overfill of accepting fiber NA and face), chromatic aberration and misalignment induced vignetting. The tolerance study indicated that +/-2 micron (1%) centration is required between the components, that is passively achieved by the opto-mechanical design (see below). This results in an overall ~80% average throughput of the scrambler, accounting for all possible losses including the AR coating.

Opto-Mechanical Realization

We worked with FiberTech Optica on the opto-mechanical design and assembly of the scrambler. To achieve the required tolerance level we decided to rely on kinematic mounting and mechanical indexing of the opto-mechanical components, and passive alignment of the fiber rotations as well as radial offset of the ball vs. fiber in one direction. In the orthogonal radial direction offset is controlled by precision lapping of a shim (see Figure 5, description below).

The fiber blocks and the ball lens support plate are kinematically mounted into an L-bracket, by positively loading them to the two perpendicular planes. The two fiber blocks are also preloaded against each other, enclosing the ball lens plate in-between the fiber blocks. (The ball plate is also preloaded against the two perpendicular surfaces of the L-bracket – for clarity this is not shown on Figure 5.). The L-bracket and the fiber blocks are made out of invar, the ball plate is stainless steel shim stock. In this assembled configuration the v-grooves are machined all at once, assuring that after disassembly and reassembly of these components the v-channels will line up. The ball plate is standing on a shim during the groove cutting, which shim is later lapped with high precision (<1μm) to de desired thickness, and so it sets the height of the ball, the radial offset between the fibers and the ball lens in the vertical direction (see Figure 5).

The next step in the assembly process is to release the fiber blocks and replace the ball plate with a thicker spacer. Then the fibers are bonded in, spanning across both blocks. The gap between the blocks is filled with soluble wax, which will

firmly grip the fibers during the next stage: cutting the fibers into two sections by a spinning diamond blade that runs across the fibers in the gap between the blocks. This way the fibers do not have to be aligned for rotation, their clocking is naturally matched and frozen. After cutting the end faces of the blocks are polished, with the fiber ends still embedded in wax, then the wax is removed. The two fiber blocks now can be placed back to the L-bracket, encapsulating the ball lens support plate, which now sits on the adjusted shim. Preloading all these components against he perpendicular surfaces of the L-bracket assures that the v-groove channels in all three components line up. The adjusted shim drops the ball lens plate by the desired amount, and so the ball lenses can be simply just dropped in place. To secure the lenses a soft retainer plate (teflon) is attached to the top of the assembly (there are 4 mounting holes for that in the fiber blocks, but for clarity the retainer plate is not shown on Figure 5). Since the balls slightly protrude above the top surface of the fiber blocks this gives a positive preload and keeps the balls in place. The retainer also protects the exposed fiber ends.

The fibers are secured to the blocks, and from there enter a braided steel conduit for protection. This conduit is secured to the L-bracket for stress relief, but also can be directly attached to the fiber block. The idea here is that the fiber blocks can be separated from the L-bracket and inserted into a protective head, which allows feeding the fiber through the telescope mount and pier. Then the scrambler can be re-assembled on site, by simply dropping the ball lenses back in under a microscope, and re-attaching the retainer plate.
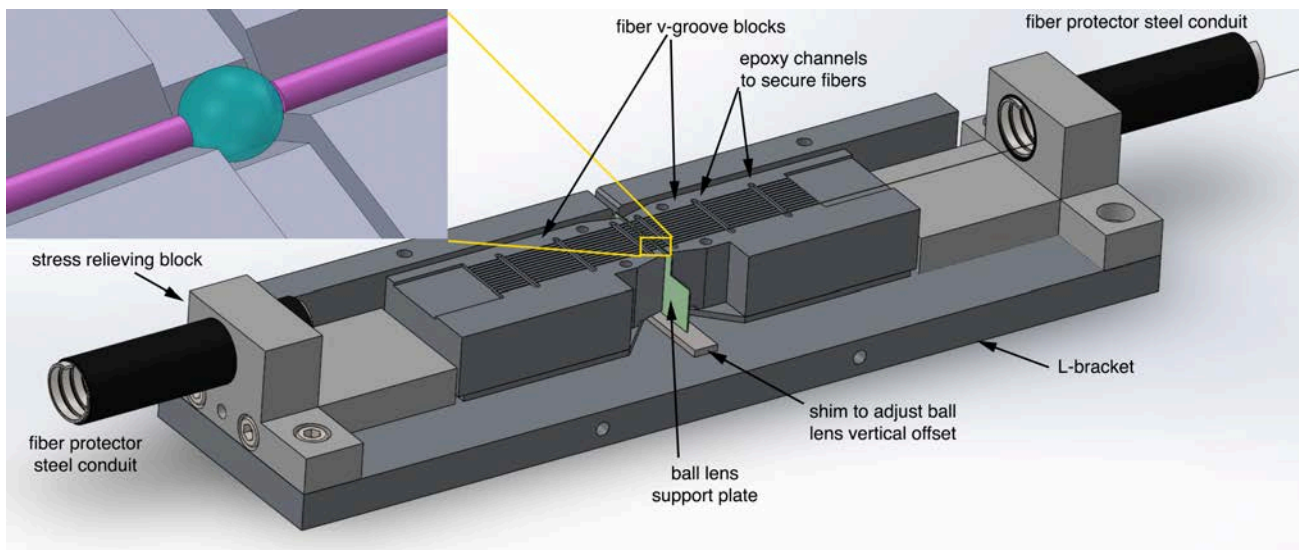

Figure 5. Opto-mechanical design of the scrambler assembly.

Alternative Realizations

Precision alignment between the ball lens and the fibers can be achieved in other ways. One solution is to custom design the fiber to have the same outer diameter as the ball lens, so the two fibers and the lens can be simply dropped into a single continuous v-groove. For our custom single-clad fiber, as mentioned above, this was really not an option. However after the preform is made its geometry can be modified by inserting the preform into a properly sized outer tube, collapsing that onto the preform and drawing a new fiber, which now can have the same outer diameter as the ball lens. Such customization of the preform can be done for about $10k, comparable to the implementation of the described mechanical assembly. While this is a very appealing solution for a simple and precise alignment it alters the preform in a non-reversible way and such large diameter could be a problem if the fiber cores need to be brought close together to form a tight slit. If the preform is long enough, though, it could be split into two and only one part altered. Still, it assumes ownership of the preform, which is not always the case.

Another solution could be mounting using a silicon wafer, onto which alignment features are machined lithographically. Such technique has sub-micron precision, and by selecting the right crystal orientation of the wafer a very simple etching mask can be used: the facets of the crystal lattice will naturally provide v-grooves and the depth of the features will be linearly proportional to the width of the exposed mask. This, coincidentally, costs roughly the same amount as the other two methods. Photo-assisted chemical etching can also provide arbitrary geometry machined into fused silica with micron precision. Companies like FEMTOprint offer affordable services and quick turnaround times, as yet another alternative for such scrambler mount.

2.4 3-to-1 Fiber Splicing – Mitigation of Modal Noise

Smaller core fibers have a correspondingly lower modal volume. The number of light propagation modes for our 32μm fiber can be estimated as:

$$M = \frac{1}{2}\left(\frac{\pi \cdot d_{\mathrm{core}} \cdot \mathrm{NA}}{\lambda}\right)^2 \approx 250\left(\frac{\lambda}{6500\text{Å}}\right)^{-2} \tag{2}$$

which is about 250 modes at the center of WISDOM's passband. This is a fairly low number, and so a single fiber would be very susceptible to modal structure and modal noise. Therefore we plan to combine 3-3 of the 6 slicer fibers and merge them into two rectangular fibers, which then each would contain ~750 modes. For comparison, HARPS employs a single 67 μm core fiber illuminated at NA=0.125, yielding 820 total modes at 0.65 μm. It is important to remember that while the HARPS fiber with its larger diameter and higher numerical aperture of 0.22 could support a lot larger number of modes, but coupling light into the fiber from the telescope at a lower NA value does not excite all the possible modes. Thus our fiber sextet should provide modal volume comparable that of HARPS, at a fixed wavelength. Still, the red end of our passband extends much further than HARPS, at 1.2μm the mode count decreases by a factor of 4 to M ~ 375 speckles per rectangular fiber.

The consequences of modal discreteness are most severe for the laser frequency comb, since it has a higher degree of coherence than seeing-modulated starlight. Employing a 30 Hz temporal scrambler (fiber agitator), located in the rectangular portion of the fiber run, and integrating over the expected exposure times (10-15 seconds even for calibration light) would yield 300-500 realizations of the speckle pattern and hence ~150,000 effective modes to average at the red end of WISDOM's passband.
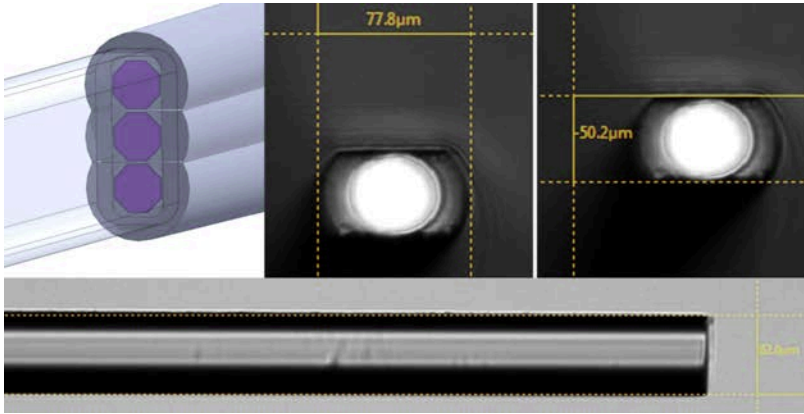

Figure 6. Layout of the 3:1 fiber splicing, with the rectangular fiber shown transparent for clarity. The octagonal fiber cores need to be brought very closely together, which is achieved by single- and double-side polishing. Tests of side polishing (on circular fibers) are shown on the upper right and bottom.
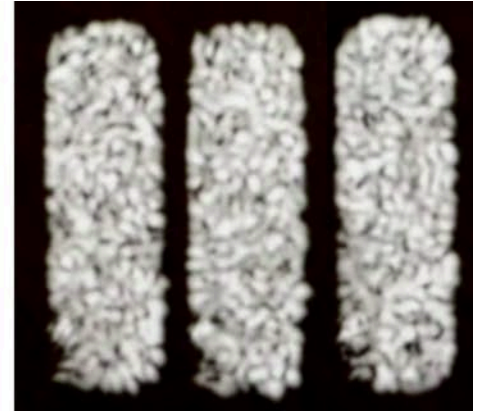

Figure 7. Three realization of modal structure in the 34x106μm rectangular fiber, illuminated by a HeNe laser (that is not properly coupled to fill the fiber NA).

2.5 Slit Architecture

The two rectangular fibers, onto which each a trio of side polished octagonal fibers are spliced using a Vytran GPX workstation, form the slit at the spectrograph. Since the emerging beam is about F/3 accounting for some FRD there is a projection optics that creates an F/8 beam matching the OAP collimator of the spectrograph. This pre-optics collimates the beam then creates a real, intermediate image of the slit, offering a possibility to clean the pupil and also to conveniently implement the high-resolution mode by a moveable slit mechanism. As seen on Figure 8 the two rectangular slit-halves are not butted to form a continuous slit, but rather surround a single 32μm octagonal calibration fiber that is illuminated directly from the calibration system. Advantage of placing the simultaneous calibration trace in between the two slit elements that this way any blooming or background contamination of a calibration line affects the same spectral order in which the calibration line
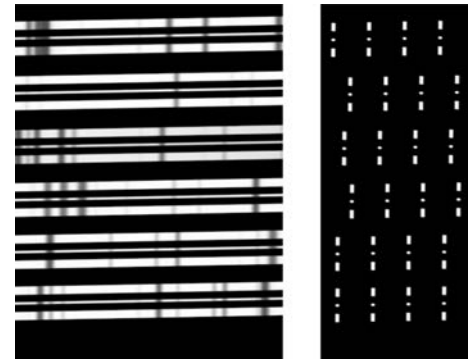

Figure 8. Simulated stellar and LFC spectrum clearly shows the slit architecture. Note the lack of slit tilt.

itself occurs, and also evenly diluting both slit traces. Therefore corrections and/or elimination for such effects are straightforward. The two-part slit also offers the possibility of cross-correlation between the two independent traces, each including very similar but not the exact same fiber run. This can help to identify potential systematics. Great care has been taken in the optical design to eliminate slit tilt, which varies only at the ±0.1° level across each echellogram. This allows binning in the cross dispersion direction without the penalty of degrading resolution. Figure 8 shows the portion of the Green echellogram where inter-order spacing is minimal. Since we chose to use 4 cameras cover the wide passband of WISDOM, the inter-order spacing is very generous even at the displayed densest region, allowing for a clear extraction and precise background subtraction. (The optical design is balanced to provide the same minimum inter-order spacing for all cameras.)
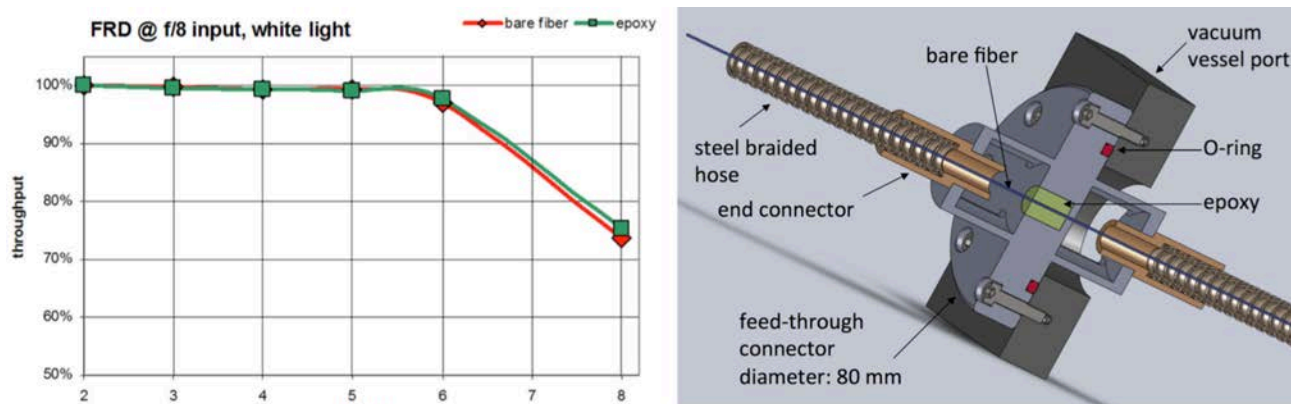

Figure 9. Vacuum feed-through design and FRD performance.

2.6 Vacuum Feed-thru

We chose a direct fiber feed-thru instead of an optical relay system, as our FRD tests (see Figure 9, left) indicated that, with care, a bare fiber can be embedded in an epoxy vacuum seal without affecting FRD performance. It is advised to use low shrinkage epoxy and/or mix the epoxy with silica powder (40-60% in weight) to match the CTE of the fiber and avoid stress induction while assembly and with changing temperature. (Although the wall of the vacuum vessel does have a <±0.1°C level temperature control[3].) The probably more important aspect is to support the epoxy plug from the inside of the chamber, by filling epoxy to encapsulate the fiber inside of a bottomed hole that only has a tiny opening for the fiber to pass through (see Figure 9, right). This way when the chamber is under vacuum the atmospheric pressure does not stress/shear the epoxy plug, and thus not induces stress and increase FRD in the fiber.

Evacuating the chamber and variations in ambient pressure also results in deformation of the vacuum vessel. This is why the optical bench on the inside needs to be kinematically supported so such deformations do not impose stress and dimensional changes onto the optical bench.[3] But in case of an optical relay coupling an external fiber end to an internal fiber component through a window, it is important to make sure that the breathing of the vessel does not displace the vessel mounted outside collimator/optical assembly respect to the internal one. Our proposed solution completely avoids this issue, and has an inherently higher throughput than an optical relay – although often such optical coupling is the location where the double scrambler is implemented, and thus it doesn't really add throughput losses to the overall efficiency.

3. COMPONENT LEVEL AND END-TO-END CHARACTERIZATION

Our PRV fiber run consists of many components and subsystems, as discussed above. Performance can be evaluated for some of these independently, but not for all. We argue that even if component level verification is available for all pieces that still does not substitute an end-to-end comprehensive testing.

Let's take for example fiber termination that can be done either by polishing or cleaving. Each has its advantages and drawbacks, but it is well know that end effects are the major contributors to FRD rather than inherent properties since those are very good for late fibers like the FBPI series. Therefore how the fiber is terminated (and mounted) is very important, while of course how the fiber is managed and protected along the fiber link does also contribute to FRD at some level. Just

looking at a microscopic image of a fiber end it is possible to judge the surface roughness to a point, but rather hard to gauge how deep and severe subsurface damage remains from polishing. Similarly difficult to evaluate under a regular microscope if the cleaving has truly been optimized, not just to avoid any cleave marks or misting on the sides, but also not to have the side-reflected and colliding stress-waves to cause sub-micron interference ripples opposing the cleave point. Certain techniques can reveal these often omitted signatures (e.g. phase contrast or dark field microscopy), but that does not really translate to an FRD measurement, which is a really meaningful measure of throughput loss in the fiber link. Directly measuring FRD over the end-treated bare fiber is more informative, but the temporal mounting and missing protective conduit might alter such measurement compared to what it really would be when the fiber is mounted at the telescope.

Another concern is that if the real refractive index profile of the particular fiber used is not known, then one cannot assume, as we have learnt the hard way, that just because it is an octagonal fiber then the near- and far field behavior would be just like someone else measured for another octagonal fiber. Elaborate laboratory characterizations go as far as modeling the telescope central obscuration, or a possibly even more complex pupil, as light is injected into the fiber under test. While this and even guiding errors (by shifting the fiber respect to the projected beam) can be feasibly well simulated, the optics used in a laboratory setting does not produce the PSF of a telescope, and thus modal coupling achieved on an optical table can be very different to that of real starlight. Not to mention that there are significant variations amongst test setups built and methods used by different groups, and without knowing all the details it is hard to objectively compare test results.

3.1 Comprehensive Fiber Test Bed

Due to these above reasons we decided to design a comprehensive fiber test station (see Figure 10), that can measure FRD, absolute throughput, near and far field performance at once, for bare fibers and for fiber assemblies as well. We teamed up with Polymicro to implement it, since they long wanted to develop such capability, but did not have the capacity to design the system. The agreement was that we develop and implement the test setup, while Polymicro purchases all the hardware components (as the awarded NASA-NSF funding was nearly not sufficient to complete the conceptual design itself, not to mention prototyping). Polymicro's plan is to use this test setup for product development and quality control, as well as to offer some sort of standardized characterization and measurement service to their customers.
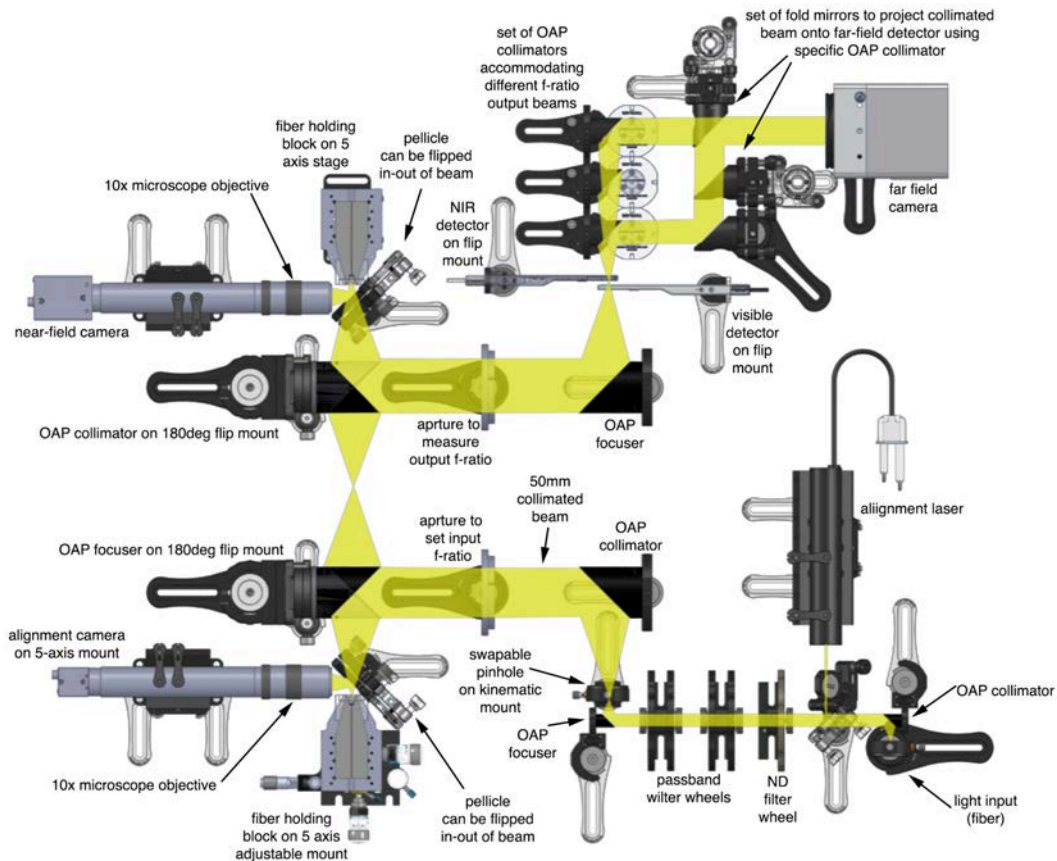

Figure 10. A comprehensive fiber test setup to evaluate FRD, throughput, near- and far field at once.

The test setup is build using COTS (mostly Throlabs) components, and it can measure FRD and throughput with very high S/N ratio and dynamic range over a 350-1200 nm passband thanks to its all-reflective optics. Near- and far field imagery is limited by the sensitivity of cameras to ~400-950nm (although the detectors can be swapped/upgraded, if necessary). The system allows dialing in narrow (5nm) passband filters at every 50nm within the above-mentioned range to evaluate wavelength dependency of FRD, throughput or scrambling efficiency. Input focal ratios of up to f/2 can be accommodated, and the NA (or f-ratio) of the input beam is easily set by a large iris. The far-field image is kept at nearly the same size for output f-ratios between f/2 and f/10 by switching of collimators, and so comparative evaluations are easy and accurate. Bare or connectorized fibers can be all tested, and alignment is easy thanks to a sighting laser and a live view camera. Telescope pupils are straightforward to simulate, as there is easy access to a pupil plane where proportionally scaled model of spider vanes, central obscuration, etc. can be placed. An atmospheric seeing simulator (e.g. Lexitek) could be also installed here. Quick swapping of kinematically mounted pinholes to desired size can easily modulate the input illumination, and the input fiber can be offset to mimic guide and focus errors.

4.SUMMARY & LESSONS LEARNED

The WISDOM fiber run is a state-of-the-art PRV oriented fiber run, that achieves high overall throughput for all 4 cameras over the wide passband of the instrument: 35-55% efficiency for the blue channel (380-480nm), 62-70% for the green (480-750nm), and 70% for the red (750-950nm) and NIR (950-1300nm) channels. These respectable throughput values include: the pupil slicer; the entire fiber run that consists of octagonal and rectangular fibers; a single ball lens double scrambler; accounting for focal ratio degradation, AR and mirror coatings and geometrical/alignment losses.

In the paper we discussed the key components of a fiber run that aims to deliver a superbly stable and very evenly illuminated near and far field to the spectrograph, independent of atmospheric and guiding errors or other environmental disturbances. If anything this is the area where PRV spectrographs can gain the most advance towards the sub-m/s precision regime, since all of these components with such attention to details have not yet been in implemented at once in a fiber run per design (except probably for the CARMENS instrument). Soon-to-be commissioned spectrographs, like ESPRESSO, HPF and EXPRES, have similarly advanced fiber systems, for the mentioned reasons.

While NASA had not selected our WISDOM concept for implementation, we think that our prototyping and design analysis has produced some useful and more widely applicable results that this paper aimed to summarize and share. The comprehensive fiber test setup we built is likely to be used by many groups ordering fibers from Polymicro; some of our design elements might be implemented (like the pupil slicer, fiber combiner); or the vendors we worked with to be used by others. We cannot emphasize enough the cautionary tale regarding fiber customization and fully thorough testing, not just of components and subsystems, but the final end-to-end product as well, in the most realistic way possible.

REFERENCES

[1] Fischer, D., G. Anglada-Escude, P. Arriagada, R. V. Baluev, J. L. Bean, F. Bouchy, L. A. Buchhave, T. Carroll, A. Chakraborty, J. R. Crepp, R. I. Dawson, S. A. Diddams, X. Dumusque, J. D. Eastman, M. Endl, P. Figueira, Eric B. Ford, D. Foreman-Mackey, P. Fournier, G. Furesz, B. S. Gaudi, P. C. Gregory, F. Grundahl, A. P. Hatzes, G. Hebrard, E. Herrero, D. W. Hogg, A. W. Howard, J. A. Johnson, P. Jorden, C. A. Jurgenson, D. W. Latham, G. Laughlin, T. J. Loredo, C. Lovis, S. Mahadevan, T. M. McCracken, F. Pepe, M. Perez, D. F. Phillips, P. P. Plavchan, L. Prato, A. Quirrenbach, A. Reiners, P. Robertson, N. C. Santos, D. Sawyer, D. Segransan, A. Sozzetti, T. Steinmetz, A. Szentgyorgyi, S. Udry, J. A. Valenti, S. X. Wang, R. A. Wittenmyer, J. T. Wright, "State of the Field: Extreme Precision Radial Velocities", arXiv: 1602.07939 (2016)

[2] Plavchan, P., D. Latham, S. Gaudi, J. Crepp, X. Dumusque, G. Furesz, A. Vanderburg, C. Blake, D. Fischer, L. Prato, R White, V. Makarov, G. Marcy, K. Stapelfeldt, R. Haywood, A. Collier-Cameron, A. Quirrenbach, S. Mahadevan, G. Anglada, P. Muirhead, "Radial Velocity Prospects Current and Future: A White Paper Report prepared by the Study Analysis Group 8 for the Exoplanet Program Analysis Group (ExoPAG)", arXiv: 1503.01770 (2015)

[3] Fűrész, G., Simcoe, R., Barnes, S. I., Buchhave, L. A., Egan, M., Foster, R., Hellickson, T., Malonis, A., Phillips, D., Shectman, S., Walsworth, R., Winn, J., and Woods, D. F., "WISDOM: the WIYN Spectrograph for DOppler Monitoring – a NASA-NSF concept for an extreme precision radial velocity instrument in support of TESS", Proc. SPIE 9908, 9908-41, these proceedings (2016).

[4] Barnes, S., G. Furesz, R. Simcoe, S. Shectman, D. F. Woods, "Optical design of the NASA-NSF Extreme Precision Doppler Spectrograph concept WISDOM", Proc. SPIE 9908-247, these proceedings (2016)

[5] Sullivan, P. W., J. N. Winn, Z. K. Berta-Thompson, D. Charbonneau, D. Deming, C. D. Dressing, D. W. Latham, A. M. Levine, P. R. McCullough, T. Morton, G. R. Ricker, R. Vanderspek, D. F. Woods , "The Transiting Exoplanet Survey Satellite: simulations of planet detections and astrophysical false positives", ApJ 809, 77 (2014)

[6] Quirrenbach, A.; Amado, P. J.; Mandel, H.; Caballero, J. A.; Mundt, R.; Ribas, I.; Reiners, A.; Abril, M.; Aceituno, J.; Afonso, C.; Barrado y Navascues, D.; Bean, J. L.; Béjar, V. J. S.; Becerril, S.; Böhm, A.; Cárdenas, M. C.; Claret, A.; Colomé, J.; Costillo, L. P.; Dreizler, S.; Fernández, M.; Francisco, X.; Galadí, D.; Garrido, R.; González Hernández, J. I.; Guàrdia, J.; Guenther, E. W.; Gutiérrez-Soto, F.; Joergens, V.; Hatzes, A. P.; Helmling, J.; Henning, T.; Herrero, E.; Kürster, M.; Laun, W.; Lenzen, R.; Mall, U.; Martin, E. L.; Martín-Ruiz, S.; Mirabet, E.; Montes, D.; Morales, J. C.; Morales Muñoz, R.; Moya, A.; Naranjo, V.; Rabaza, O.; Ramón, A.; Rebolo, R.; Reffert, S.; Rodler, F.; Rodríguez, E.; Rodríguez Trinidad, A.; Rohloff, R. R.; Sánchez Carrasco, M. A.; Schmidt, C.; Seifert, W.; Setiawan, J.; Solano, E.; Stahl, O.; Storz, C.; Suárez, J. C.; Thiele, U.; Wagner, K.; Wiedemann, G.; Zapatero Osorio, M. R.; del Burgo, C.; Sánchez-Blanco, E.; Xu, W., "CARMENES: Calar Alto high-resolution search for M dwarfs with exo-earths with a near-infrared Echelle spectrograph", Proc. SPIE 7735, 773513 (2010)

[7] Hunter, T.R., and Ramsey, L.W., "Scrambling properties of optical fibers and the performance of a double scrambler", PASP 104, 1244 (1992)

[8] Chazelas, B., Pepe, F., Wildi, F., Bouchy, F., Perruchot, S., and Avila, G., "New scramblers for precision radial velocity: square and octagonal fibers" , Proc. SPIE 7739, 773947(2010)

[9] Avila, G. "FRD and scrambling properties of recent non-circular fibres", Proc. SPIE 8446, 84469L (2012)

[10] Boisse, I., Bouchy, F., Chazelas, B., Perruchot, S., Pepe, F., Lovis, C., and Hebrard, G., "Consequences of spectrograph illumination for the accuracy of radial-velocimetry," arXiv 1001.0794 (Jan. 2010).

[11] Chazelas, B., Pepe, F., Wildi, F., "Optical fibers for precise radial velocities: an update", Proc. SPIE 8450, 845013 (2012)

[12] Ramsey, L. W., Brown, T. M., Gilliland, R. L., and Noyes, R. W., "A new technique for study of radial velocity changes", 1989, ASPC 20, 614 (1991)

[13] Halverson, S., A. Roy, S. Mahadevan, L. Ramsey, E. Levi, C. Schwab, F. Hearty, N. MacDonald, "An efficient, compact, and versatile fiber double scrambler for high precision radial velocity instruments", ApJ 806, 61 (2015)

[14] Bouchy, F., Pepe, F., Queloz, D., "Fundamental photon noise limit to radial velocity measurements", Astronomy and Astrophysics v.374, p.733-739 (2001).

[15] Barnes, S. I., and MacQueen, P. J., "A high-efficiency fibre double-scrambler prototype", Proc. SPIE 7735, 773567 (2010)

[16] Li, C.-H., A. Glenday, A. Benedick, G. Chang, L.-J. Chen, C. Cramer, P. Fendel, G. Furesz, F. Kaertner, S. Korzennik, D. Phillips, D. Sasselov, A. Szentgyorgyi and R. Walsworth. In-situ determination of astro-comb laser calibrator lines to beetter than 10 cm s-1, Opt. Express 18, 13239-13249 (2010)

[17] Phillips, D. F., A. Glenday, C-H. Li, G. Furesz, A. J. Benedick, G. N. Chang, L-J. Chen, S. Korzennik; D. Sasselov; F. X. Kaertner; A. Szentgyorgyi; R. L. Walsworth, "Calibration of an Echelle Spectrograph with an Astro-Comb: a Laser Frequency Comb with Very High Repetition Rate.", Proc. SPIE 8446, 84468O (2012)

[18] Egan. M., G. Fűrész, R. Foster, R. Simcoe, "Pupil slicer design for the NASA-NSF Extreme Precision Doppler Spectrograph concept WISDOM", Proc. SPIE 9912-183, these proceedings (2016)

[19] Seifahrt, A., Stürmer, J., Bean J. L., "A micro-lens array based pupil slicer and double scrambler for MAROON-X", Proc. SPIE 9908, 9912-61, these proceedings (2016)

[20] Avila, G., Singh, P., and Chazelas, B., "Results on fibre scrambling for high accuracy radial velocity measurements", Proc. SPIE 7735, 773588 (2010)